Localization of Vibrations in Large Space Reflectors

Phillip J. Cornwell* and Oddvar O. Bendiksen†
Princeton University, Princeton, New Jersey

A study is presented of the mode localization phenomenon in a generic class of large space reflectors. The study is based on a Rayleigh-Ritz formulation using the first five cantilevered beam bending modes and a finite-element formulation using Bernoulli-Euler beam elements. Coupling between the structures is provided by massless axial members. Numerical results indicate that mode localization does, in fact, occur in engineering structures of this type. Localization is characterized by the amplitude of a global mode becoming confined to a local region of the structure. For the 18-rib reflector studied, the first rib bending mode did not localize, but the second and third modes did. Localization is found to become more severe with increasing mode number. Increasing the number of ribs to 48 resulted in significant distortion in some of the first rib bending modes and severe localization of the second and third bending modes. The phenomenon of wave confinement in finite structures is also demonstrated using a single-degree-of-freedom per substructure model.

Nomenclature

A = cross-sectional area of axial member
EI = rib flexural rigidity
k_{ij}^a = effective stiffness of axial member
$[K]$ = global stiffness matrix
ℓ = total length of rib
ℓ_a = length of axial member
m = rib mass per unit length
$[M]$ = global mass matrix
n = circumferential wave number
N = total number of ribs
N_a = number of axial members connecting ribs
N_e = number of beam elements per rib
p = number of degrees-of-freedom per substructure
q_i = generalized coordinate
Q_i = generalized force
$\bar{q}_i$ = amplitude of q_i
t = time
T = total kinetic energy
U = total potential energy
$v(x,t)$ = displacement of in-plane motion
V_{ij} = potential energy due to jth axial member between rib i and $i+1$
$w(x,t)$ = displacement of out-of-plane motion
$\bar{x}$ = x/ℓ
α = cone angle
β_i, α_i = constants in assumed mode shapes
θ = half-angle between ribs
λ = $(\omega/\omega_0)^2$ = eigenvalue
ω = natural frequency
ω_0 = $\sqrt{EI/m\ell^4}$ = reference frequency
$\bar{\omega}$ = ω/ω_0 = nondimensional frequency
$\Delta\bar{\omega}^2$ = normalized eigenvalue band
$\phi_n(x)$ = mode shape function

Presented as Paper 87-0949 at the AIAA Dynamics Specialists Conference, Monterey, CA, April 9-10, 1987; received Nov. 24, 1987; revision received June 8, 1988.

*Graduate Student, Department of Mechanical and Aerospace Engineering.
†Assistant Professor, Department of Mechanical and Aerospace Engineering.

Introduction

PROPOSED designs for large space structures have explored a number of different ways of constructing complex structures from relatively simple substructures. The assembly is then periodic or cyclic in one or more dimensions, and efficient methods have been developed for analyzing such structures (see, for example, Ref. 1).

In a number of recent investigations,[2-6] periodic structures have been shown to be sensitive to certain types of imperfections or disorder. When imperfections break the periodicity of the structure, some of the natural modes of vibration may become confined to a local region of the structure. In applications where accurate shape control is required, such as in large astronomical telescope reflectors and communication antennas, the presence of localized vibrations would obviously be undesirable. Also, because the regular features of the original mode are destroyed, the new mode shape would, in all likelihood, be misidentified, and the mode may no longer be controllable.

This paper is a continuation and extension of the investigation initiated in Ref. 5, where the possibility of mode localization in large space structures was studied from a fundamental point of view. It was found that structures consisting of a large number of weakly coupled substructures are especially susceptible to mode localization. Preliminary calculations indicated that large disk antennas and reflectors of the type analyzed in Ref. 7 could exhibit localized modes.

The objective of the present paper is to extend the study of Ref. 5 to multi-degree-of-freedom (DOF) substructures, using Rayleigh-Ritz and finite-element formulations. A systematic study of localization is carried out for a generic class of reflectors, and some of the important predictions of localization theory are verified through numerical simulations. To our knowledge, this represents the first time that conclusive and definite numerical results have been presented to show that the confinement phenomenon does, in fact, occur in engineering structures of this type.

Structural Models

For the class of axially symmetric reflector and antenna structures considered in this study (Fig. 1), the basic substructure consists of one of the N radial beams (ribs) with the associated wire mesh (Fig. 1b). Two different structural models are used: a Rayleigh-Ritz model based on the first five cantilever beam bending modes for each radial rib, and a finite-element model based on N_e standard Bernoulli-Euler

beam elements per rib. The number of elements N_e can be varied to ensure that all modes of interest are resolved to sufficient accuracy, and also to permit the modeling of radial variations (nominal and imperfections) in beam mass and stiffness. In both models, the wire mesh or web membrane between the ribs is modeled as a number of massless axial members (springs) attached at specific points, and the hub of the reflector is considered fixed, as illustrated in Fig. 1.

For small-amplitude vibrations and a cone angle of zero, in-plane and out-of-plane vibrations decouple and can, therefore, be considered separately. The vibration displacement of the beam in the plane of the reflector is denoted by $v_i(x,t)$, and the corresponding out-of-plane displacement is denoted by $w_i(x,t)$ (Fig. 1c). In the structures studied in Refs. 7 and 8, the ribs are oriented with their weaker flexural rigidity about the z axis; thus, the rib in-plane modes have lower frequencies than the corresponding out-of-plane modes.

Rayleigh-Ritz Model

For the Rayleigh-Ritz model, the in-plane displacement of a rib can be written as

$$v_i(x,t) = \sum_{n=1}^{5} q_n(t)\phi_n(x) = \{q\}_i^T\{\phi\} \tag{1}$$

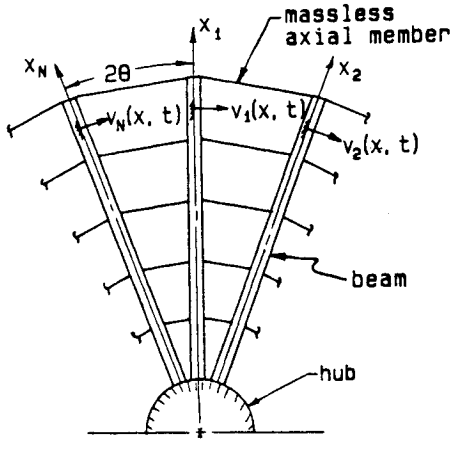

Fig. 1a Structural model for radial rib reflector/antenna.

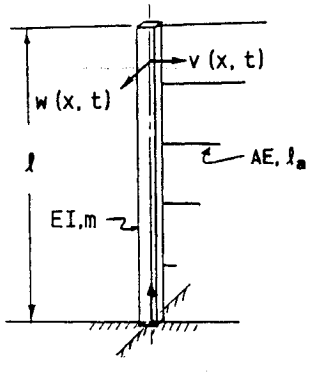

Fig. 1b Typical substructure, consisting of rib beam and sectional wires (axial members).

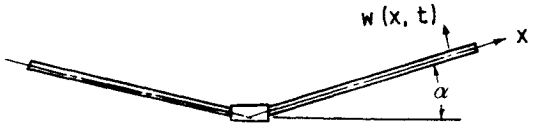

Fig. 1c Cone angle α.

The mode shape used in this study is given by

$$\phi_n = \cosh\beta_n\bar{x} - \cos\beta_n\bar{x} - \alpha_n(\sinh\beta_n\bar{x} - \sin\beta_n\bar{x}) \tag{2}$$

where

$$\begin{aligned} \beta_1 &= 1.875104 & \alpha_1 &= 0.7340955 \\ \beta_2 &= 4.694091 & \alpha_2 &= 1.018466 \\ \beta_3 &= 7.854757 & \alpha_3 &= 0.9992245 \\ \beta_4 &= 10.99554 & \alpha_4 &= 1.000034 \\ \beta_5 &= 14.13717 & \alpha_5 &= 0.9999986 \end{aligned} \tag{3}$$

The total kinetic energy is

$$T = \sum_{i=1}^{5} T_i = \sum_{i=1}^{5} \tfrac{1}{2}\{\dot{q}\}_i^T[M]_i\{\dot{q}\}_i \tag{4}$$

where

$$[M]_i = \int_0^{\ell} m_i\{\phi\}\{\phi\}^T\,dx \tag{5}$$

The total potential energy can be written as a sum of the strain energy due to bending of the beams and the strain energy in the axial members between the beams:

$$U = \sum_{i=1}^{N} \tfrac{1}{2}\{q\}_i^T[k]_i\{q\}_i + \sum_{i=1}^{N}\sum_{j=1}^{N_a} V_{ij} \tag{6}$$

where

$$[k]_i = \int_0^{\ell} (EI)_i\{\phi''\}\{\phi''\}^T\,dx \tag{7}$$

$$V_{ij} = \tfrac{1}{2}(AE/\ell_a)_{ij}\cos^2\theta\,[v_i(h_j,t) - v_{i+1}(h_j,t)]^2 \tag{8}$$

$$= \tfrac{1}{2}k_{ij}^a(\{q\}_i^T\{\phi\}|_{h_j} - \{q\}_{i+1}^T\{\phi\}|_{h_j})^2 \tag{9}$$

$$k_{ij}^a \equiv (AE/\ell_a)_{ij}\cos^2\theta \tag{10}$$

Here, k_{ij}^a is the effective stiffness of the jth spring between beams i and $i+1$. The equations of motion can be obtained by substituting Eqs. (4-10) into Lagrange's equations, resulting in a system of $5N \times 5N$ equations

$$[M]\{\ddot{q}\} + [K]\{q\} = \{Q\} \tag{11}$$

where

$$\{q\}^T = (\{q\}_1^T|\{q\}_2^T|\ldots|\{q\}_N^T) \tag{12}$$

and $\{Q\}$ is the vector of generalized forces. For small-amplitude free vibration, one can assume simple harmonic motion $\{q\} = \{\bar{q}\}e^{i\omega t}$, which, when substituted into Eq. (11), leads to the well-known structural eigenvalue problem:

$$[\bar{K}]\{\bar{q}\} = \bar{\omega}^2[\bar{M}]\{\bar{q}\} \tag{13}$$

where $\bar{\omega}^2 = (\omega/\omega_0)^2$; $\omega_0^2 = (EI/m\ell^4)_{\text{ref}}$, and $[\bar{K}]$ and $[\bar{M}]$ are the nondimensional stiffness and mass matrices, respectively.

The derivation of the equations for the out-of-plane motion is identical to the formulation for the in-plane motion, except that the effective spring stiffness given by Eq. (10) will be different. With a cone angle of zero, the out-of-plane coupling will be provided by the pretension T_0. The potential energy of the axial members can be written as

$$V_{ij} = (T_0/\ell_a)_i[w_i(h_j,t) - w_{i+1}(h_j,t)]^2 \tag{14}$$

so that the effective spring stiffness is

$$k_{ij}^{a} = (T_0/\ell_a)_i \qquad (15)$$

Because only the low-frequency in-plane modes are reported on in Ref. 7, we shall restrict ourselves to the in-plane modes in the numerical calculations.

Finite-Element Model

Standard Bernoulli-Euler beam elements using cubic Hermitian polynomials are used to model the ribs of the reflector. The coupling between ribs is provided by one or more standard axial elements. The elemental matrices can be found in any finite-element text (see Ref. 9, for example.) The global matrices are assembled using the direct stiffness method, resulting in a set of equations of the form of Eq. (11). Assuming simple harmonic motion results in a generalized eigenvalue problem in the form of Eq. (13).

The eigenvalue problems obtained from both structural formulations are solved using the IMSL subroutine EIGZS to obtain the eigenvalues and eigenvectors. When the structure is not perfectly periodic due to a random variation in one or more of the various parameters, the entire $N_p \times N_p$ eigenvalue problem needs to be solved, where p is the number of DOF substructure. For the perfect structure, the block circulant nature of the matrices enables one to reduce the order of the eigenvalue problem that needs to be solved to $p \times p$. (See Ref. 5 for a complete discussion of the reduction procedure.)

Localized Modes and Wave Confinement

The subject of eigenvector localization in disordered systems has been studied extensively over the past three decades. Because the theory had its inception in solid state physics, the best understood models are derivatives of the original Anderson model for a one-electron disordered lattice. In the one-dimensional case with next-neighbor interactions only, the Schrödinger wave equation for the electron can be written in nondimensional form as[10]

$$i\dot{a}_n = \epsilon_n a_n + V(a_{n-1} + a_{n+1}) \qquad n = 1,2,\ldots \qquad (16)$$

where a_n is the probability amplitude and ϵ_n the site energy of an electron at the nth site, and V is the transfer energy between nearest neighbor sites. Disorder is introduced by assuming that the ϵ_n are independent random variables with some given probability distribution.

Because the coordinates a_n in Eq. (16) do not have the same physical significance as generalized coordinates in structural dynamics, it is not clear what (if any) significance the electron model should have in vibration problems. However, if one considers a set of masses m_n coupled together via springs K to form a one-dimensional chain, one obtains the equation of motion

$$m_n\ddot{q}_n = K(q_{n-1} + q_{n+1} - 2q_n) \qquad n = 1,2,\ldots \qquad (17)$$

where q_n is the displacement of the nth mass from its equilibrium position. On assuming simple harmonic motions, it is clear that Eqs. (16) and (17) are of the same tridiagonal form and would admit the same types of solutions.

Equation (17) has been studied extensively in the context of lattice dynamics, where it models the vibrations of a one-dimensional atomic chain. Isotopic disorder can be introduced by making the masses m_n of the atoms be random variables. The result is a so-called isotopically disordered harmonic chain, which has been studied by a number of investigators.[10,11,13-15] It is of interest in localization theory both because of its obvious similarity to the electron model, Eq. (16), and also because it can serve as a simple model for certain periodic structures. The model can also be extended to include coupling beyond next neighbors (see, for example, Fig. 2 and the discussion of this model in Ref. 5). For a review of localization studies in one-dimensional models, see Ishii.[11]

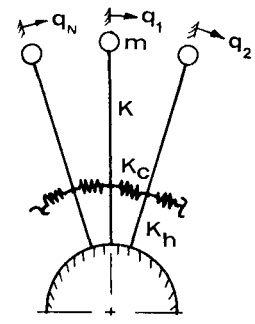

Fig. 2a Simple model of a structure with cyclic symmetry (from Ref. 5).

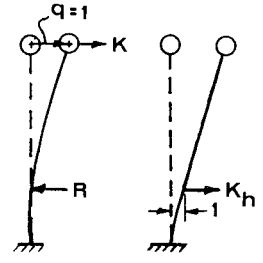

Fig. 2b Substructure (beam) stiffness coefficients.

Localization in one-dimensional systems is believed to be a consequence of the "exponential growth property" of particular solutions, as first established by Borland[12] for an electron in a disordered harmonic potential. The same behavior is exhibited by Eq. (17); i.e., one can show that the envelope of the solution grows like $\exp[\gamma(\omega)s]$, where s is the distance from the end where the boundary condition $q = 0$ is enforced, and $\gamma(\omega)$ is a positive exponent depending on ω. Borland interpreted the exponential growth property to imply that the eigenfunction must be localized with its envelope decaying exponentially on either side of a relatively small region. The exponent γ is often referred to as the degree of localization, and the inverse $1/\gamma$ defines a typical decay length scale of the eigenfunction. Other length scales characterizing the eigenfunction decay have also been proposed (see, for example, Refs. 14 and 15).

Hirota[13] has given an approximate calculation of the exponent γ for the mass-disordered harmonic chain, Eq. (17). By assuming that the masses are distributed with a sufficiently sharp maximum at the mean $\langle m \rangle$, so that moments higher than the second can be neglected, he obtains

$$\gamma(\omega) = \frac{1}{2}\lim_{n\to\infty}\left\langle \ell_n \left| \frac{q_{n+1}}{q_n} \right|^2 \right\rangle$$

$$= \frac{(\langle m^2 \rangle - \langle m \rangle^2)\omega^2}{8\langle m \rangle K(1 - \langle m \rangle \omega^2/4K)}$$

$$(1 - \langle m \rangle \omega^2/4K > 0) \qquad (18)$$

where $\langle \cdot \rangle$ denotes the average of a quantity. Note that γ is positive and proportional to the variance of m.

For realistic finite-element or Rayleigh-Ritz models of engineering structures, the mass and stiffness matrices are not necessarily tridiagonal, and the preceding results do not apply. Also, all engineering structures are *finite,* and one should therefore be careful when interpreting theoretical results derived for an *infinite* structure. At the present, most questions regarding localization in engineering structures can only be answered through numerical simulations, and that is precisely the approach followed in this paper.

Localization of eigenfunctions, or normal modes in vibration problems, leads to the surprising phenomenon of wave confinement. If one of the rib substructures in the reflector model (Fig. 1) is excited (e.g., by control forces), then one

would expect the excitation to propagate throughout the entire structure, attenuated only by structural damping. One can think of this process as the spreading out of the envelope of a "wave packet" located at the site of the original excitation. This is, in fact, what is observed in the perfectly periodic structure. But in the disordered structure, the wave packet becomes trapped around the original excitation site if the disorder to interstructural coupling ratio is sufficiently high. This phenomenon can best be explained by transferring Eq. (11) to normal coordinates η_j

$$\ddot{\eta}_j + 2\zeta_j\omega_j\dot{\eta}_j + \omega_j^2\eta_j = \{\phi\}_j^T\{Q\} \tag{19}$$

where $\{\phi\}_j$ is the jth normal mode vector, normalized with respect to the mass matrix, and ω_j, ζ_j are its frequency and damping ratio, respectively. For simplicity, consider the simple structure shown in Fig. 2, where each substructure is modeled with a single DOF q_n. If a harmonic force $Q_1 = \bar{Q}_1 \cdot e^{i\omega t}$ is applied to the first substructure, the steady-state response at the nth substructure is

$$q_n(t) = \sum_{j=1}^{N} \frac{\phi_1^{(j)} \cdot \phi_n^{(j)}}{\omega_j^2 + 2i\zeta_j\omega_j\omega - \omega^2} \cdot \bar{Q}_1 e^{i\omega t} \tag{20}$$

where $\phi_i^{(j)}$ denotes the ith component of the jth normal mode vector. If all of the eigenvectors are localized, the products $\phi_1^{(j)} \cdot \phi_n^{(j)}$ in Eq. (20) will be exponentially small for $n \gg 1$, and the nth substructure will remain (virtually) unexcited for all t. Conversely, if the eigenvectors are extended, one can readily show that all of the substructures eventually become excited, as long as the excitation frequency ω falls within one of the passbands of the structure.

Numerical Results and Discussion

In Ref. 5, the basic characteristics of mode localization were illustrated using a simple model with a single DOF per substructure, as shown in Fig. 2. The structural coupling between the substructures was modeled by springs K_c, and hub springs K_h were introduced to extend the structural coupling beyond next neighbors. Based on theoretical arguments, which were verified through numerical calculations, it was shown that structures with relatively weak coupling between the substructures, $K_c/K \ll 1$, would be most susceptible to mode localization.

Large space reflectors and antennas with many radial ribs, weakly coupled through a wire mesh or membranes, represent an important class of such structures. The narrow frequency bands of the 15-m-diam, 18-rib antenna studied in Ref. 7 are indicative of a weak coupling between the ribs. A preliminary search for localized modes in Ref. 5, using the simple structural model shown in Fig. 2, gave inconclusive results for the 18-rib antenna. However, when the number of ribs was increased to 48, localized modes did appear.

Mode Localization

Illustrative results for the 18-rib antenna are shown in Figs. 3–7, using the present improved Rayleigh-Ritz formulation with five rib bending modes. In these figures, the tip displacements of the ribs are plotted for different levels of random imperfections in the rib flexural rigidity. The imperfection strengths shown are the limits of $\Delta EI/EI$. A uniform probability distribution was used. The stiffness of the wire mesh was selected such that the frequency vs circumferential wave number n of the first in-plane rib bending mode matched the corresponding mode in Ref. 7. This resulted in an effective stiffness of $k^a = 0.298\ EI/\ell^3$. A comparison of the frequency matching is shown in Table 1. Clearly, the basic frequency behavior vs n is captured very well, despite the fact that rib curvature is accounted for in Ref. 7 but neglected in our model.

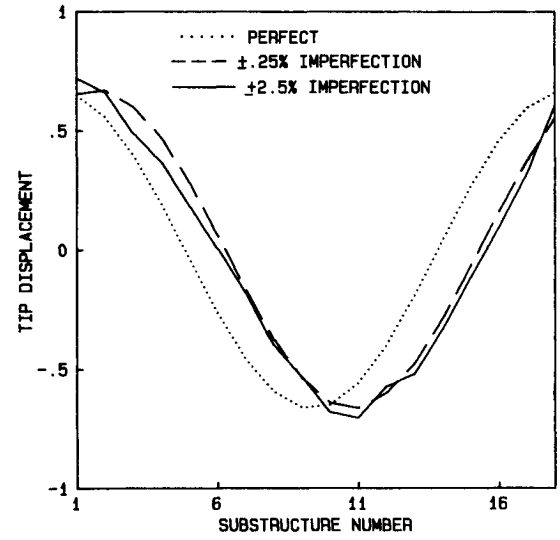

Fig. 3 Effect of imperfections on the $n = 1$ mode of the first mode group, illustrating the absence of localization. (Random imperfections in rib flexural rigidities, with uniform probability within indicated limits).

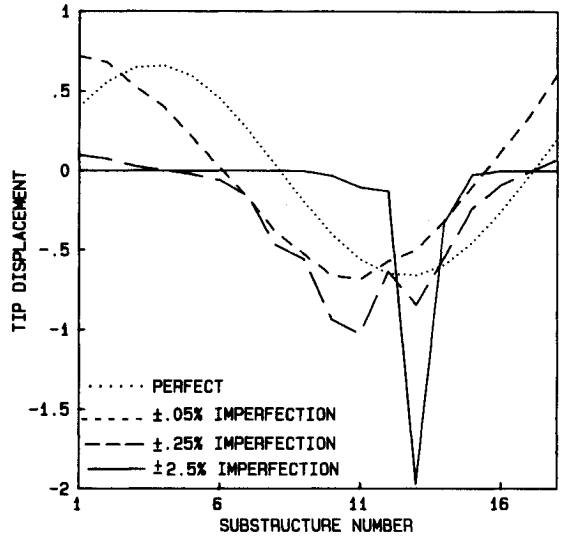

Fig. 4 Same as Fig. 3, for the second mode group, illustrating localization of mode.

The Rayleigh-Ritz model was found to provide higher accuracy with fewer DOF per rib than the finite-element model. A comparison of the normalized frequency of the $n = 0$ mode and the $n = 9$ mode, using the Rayleigh-Ritz program and the finite-element program, is shown in Table 2. The $n = 0$ mode provides a convenient check, because the exact frequencies in this case are independent of the coupling and, therefore, equal to the isolated beam frequencies. The natural frequencies were found to be clustered in mode groups. In the first mode group, the ribs are primarily in first bending. Similarly, the ribs in the second and third mode groups are primarily in second and third bending, respectively.

The results shown in Figs. 3–5 reveal two interesting aspects of the localization phenomenon. First, not all modes are susceptible. Figure 3 shows that the $n = 1$ mode of the first mode group does not localize for the imperfection strengths considered; it simply suffers slight distortion. Note that a tenfold increase in the imperfection strength, from ±0.25 to ±2.5%, does not alter the mode much. The modes in the second and third mode groups with the same circumferential

wave number ($n=1$) do exhibit localization, as shown in Figs. 4 and 5.

Second, modes that are susceptible to localization are very sensitive to relatively small levels of imperfections, and undergo drastic shape changes with increasing imperfection strengths, as is apparent from Figs. 4 and 5. In this structure, the sensitivity to imperfections clearly increases with mode number. The normalized eigenvalue bandwidth

$$\Delta\lambda_i = \Delta\bar{\omega}_i^2 \overset{\mathrm{d}}{=} (\omega_{\max}^2 - \omega_{\min}^2)/\omega_{\min\, i\ \text{fixed}}^2$$

was proposed in Ref. 16 as a measure of the effective coupling strength for a particular mode group, $i=1$ to 5. A value of $\Delta\bar{\omega}_i^2$ close to zero would indicate that the modes belonging to that group would be sensitive to imperfections and might localize. For the three modes shown in Figs. 3–5 for the perfect case, we find the following: for mode 1, $\Delta\bar{\omega}_1^2=0.3812$; for mode 2, $\Delta\bar{\omega}_2^2=0.0099$; and for mode 3, $\Delta\bar{\omega}_3^2=0.00126$. These values of $\Delta\bar{\omega}_i^2$ indicate that the third mode is almost eight times more sensitive than the second mode. Comparing Figs. 4 and 5 confirms this observation. For example, whereas the second mode is localized at an imperfection strength of $\pm$ 2.5%, the third mode is fully localized at the incredibly low imperfection level of $\pm 0.25\%$. Figure 6 shows that a further tenfold increase in the imperfection strength, to $\pm 2.5\%$, does not change the mode appreciably.

In calculating the results shown in Figs. 3–6, the coupling between the reflector ribs was modeled with a single preloaded wire, connected between the tips of the ribs. Results from calculations indicate that the use of multiple connecting wires does not change the overall behavior significantly, provided that the effective coupling strength remains the same. Figure 7 shows the results of calculations for the $n=2$ mode in the second mode group, where five equally spaced wires run circumferentially between the ribs (see Fig. 1). Localization is clearly evident when random imperfections of $\pm 2.5\%$ are introduced.

Results for a 48-rib reflector are shown in Figs. 8 and 9. The same coupling stiffness used in the 18-rib reflector was used in the 48-rib reflector. Figure 8 shows that the $n=1$ mode of the first mode group suffers significant distortion, in contrast to the slight distortion observed in the 18-rib case shown in Fig. 3. The modes in the second and third mode groups, with the same circumferential wave number, were highly localized. The $n=1$ mode of the second mode group is shown in Fig. 9. This mode and the $\pm 2.5\%$ imperfection case in Fig. 4 have essentially the same natural frequency and localize at the same ribs. The first 18 ribs of the 48-rib reflector had the same distribution of imperfections as the ribs in the 18-rib reflector. Because of this, 16 of the localized modes and natural frequencies for the second and third mode groups that appear

Table 1 Natural frequencies (Hz) of the first rib in-plane bending mode of the 15-m (18-rib) reflector vs circumferential wave number n

n	El-Raheb and Wagner[7]	Present model[a]	Difference
0	3.7590	3.7590	0%
1	3.7813	3.7808	0.013%
2	3.8440	3.8428	0.031%
3	3.9367	3.9355	0.030%
4	4.0465	4.0461	0.010%
5	4.1594	4.1601	−0.016%

[a]Rayleigh-Ritz.

Table 2 Comparison of calculated normalized frequencies ω/ω_0 for the 18-rib reflector, using the Rayleigh-Ritz and finite-element models

Bending mode	Rayleigh-Ritz[a]		Finite-Element[b]		Exact
	$n=0$	$n=9$	$n=0$	$n=9$	$n=0$
1	3.51601	4.13211	3.51601	4.13223	3.51601
2	22.0345	22.1433	22.0602	22.1693	22.0345
3	61.6972	61.7359	62.1749	62.2143	61.6972
4	120.902	120.922	122.548	122.677	120.902
5	198.860	199.871	228.137	228.149	198.860

[a]Five modes, Eq. (1); five degrees-of-freedom (DOF) per rib; 90 DOF total.
[b]$N_e=4$; eight DOF per rib; 144 DOF total.

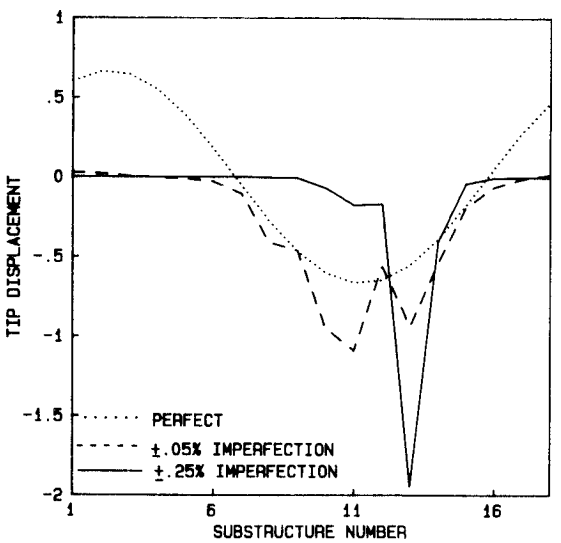

Fig. 5 Same as Fig. 3, for the third mode group, illustrating severe localization at very low imperfection levels.

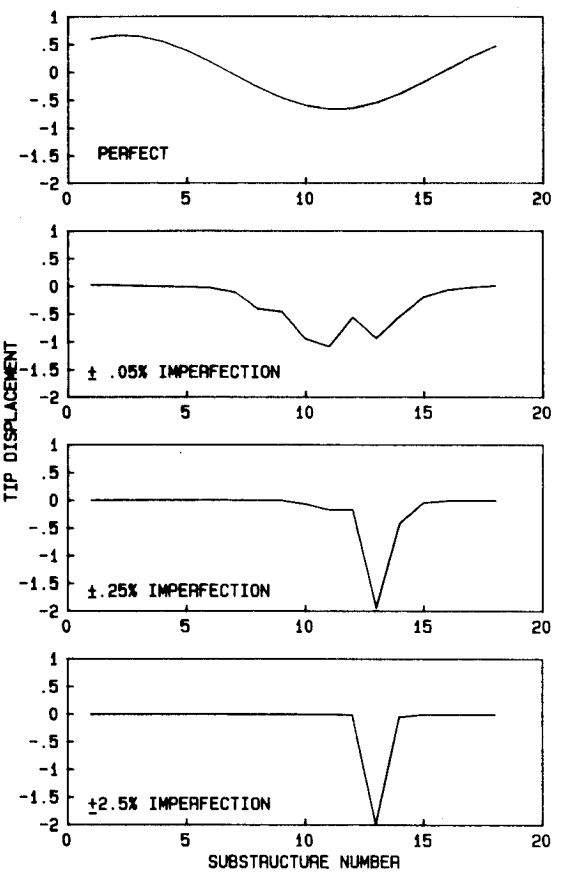

Fig. 6 Progressive localization of the $n=1$ mode in the third mode group, with increasing imperfection strength. Note that the mode is fully localized at the very low imperfection level of $\pm 0.25\%$ and changes little thereafter.

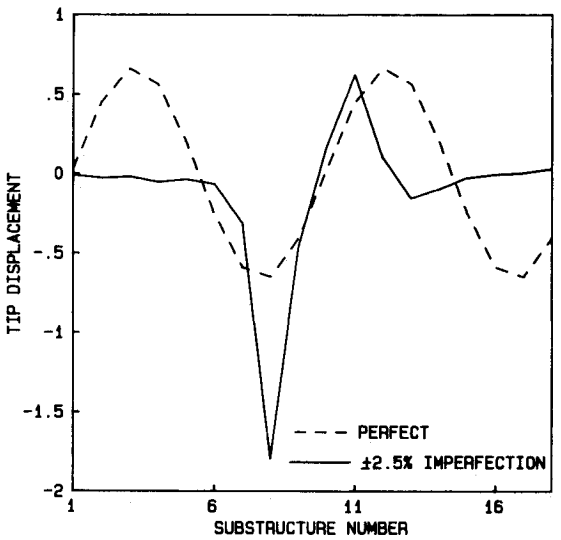

Fig. 7 Localization of the $n=2$ mode of the second mode group. Calculations based on structural model with five equally spaced axial members between each rib.

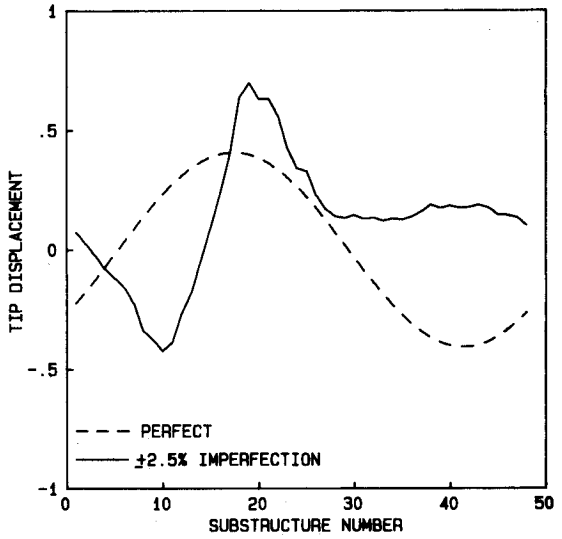

Fig. 8 Effect of imperfections on the $n=1$ mode of the first mode group for the 48-rib reflector.

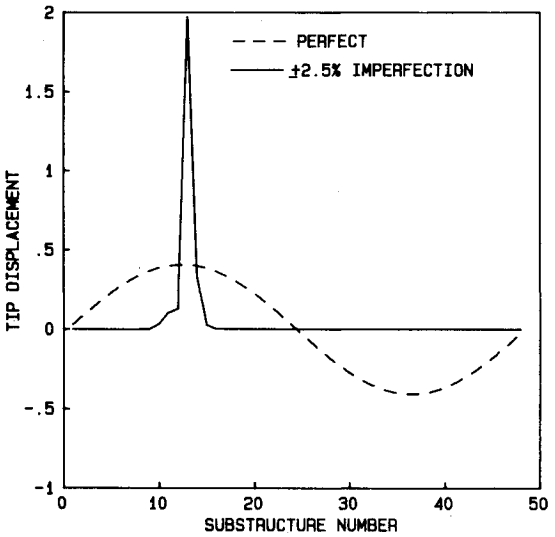

Fig. 9 Effect of imperfections on the $n=1$ mode of the second mode group, illustrating localization of mode.

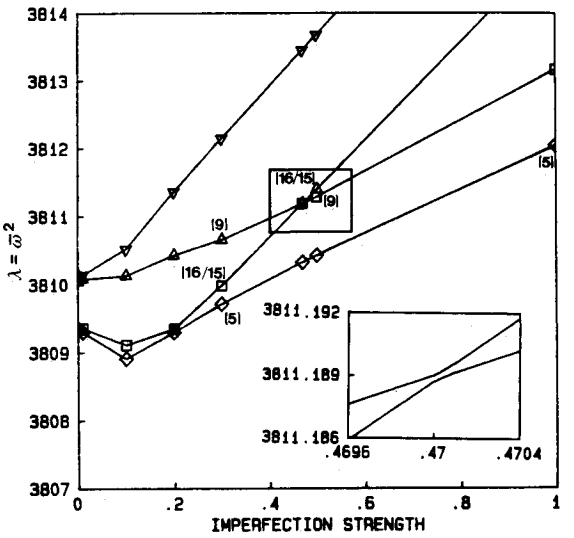

Fig. 10 Veering of frequencies of the $n=5$ and $n=6$ modes of the third group when the imperfection strength is increased. Numbers in brackets indicate the location of the peak in the associated natural mode.

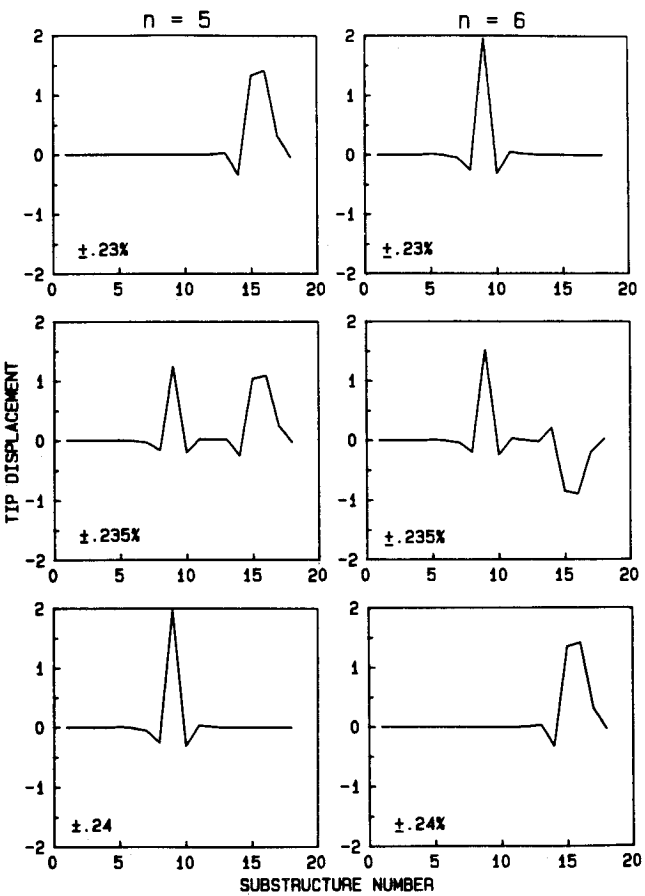

Fig. 11 Mode shapes of the $n=5$ and $n=6$ modes of the third mode group at imperfection strengths near the veering point shown in Fig. 10.

in the 18-rib case also appear in the 48-rib case, with essentially identical frequencies and mode shapes. The two modes that did not also appear in the 48-rib reflector are ones in which the localized mode involved both the first and 18th rib in the 18-rib reflector. This result indicates that, if a mode is localized, adding more ribs beyond the localized region will not affect that mode.

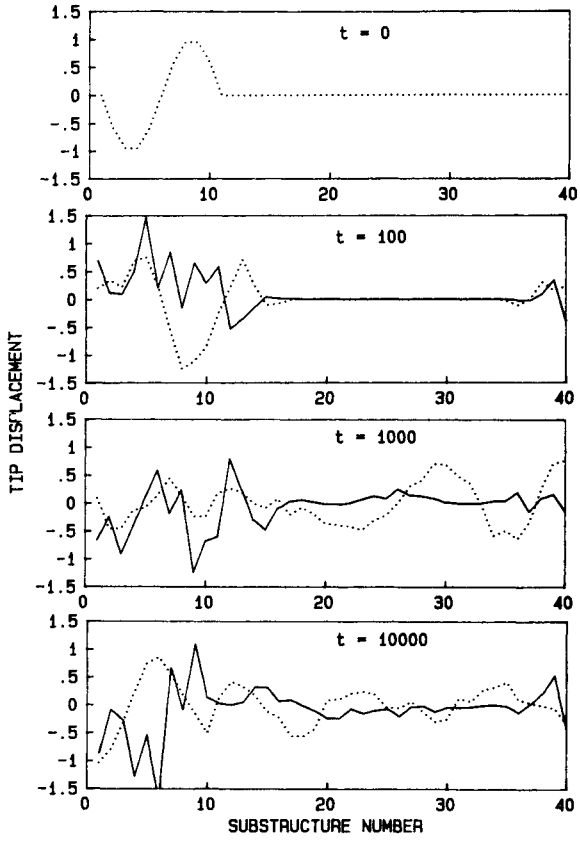

Fig. 12 Confinement of vibrational energy by structural irregularities. Original local wave packet traveling right eventually becomes distributed over entire structure if the structure is perfectly periodic (dotted line). When the structure is imperfect (solid line = ±2.5% imperfections in K), the spreading of the wave packet is strongly attenuated ($N = 40$).

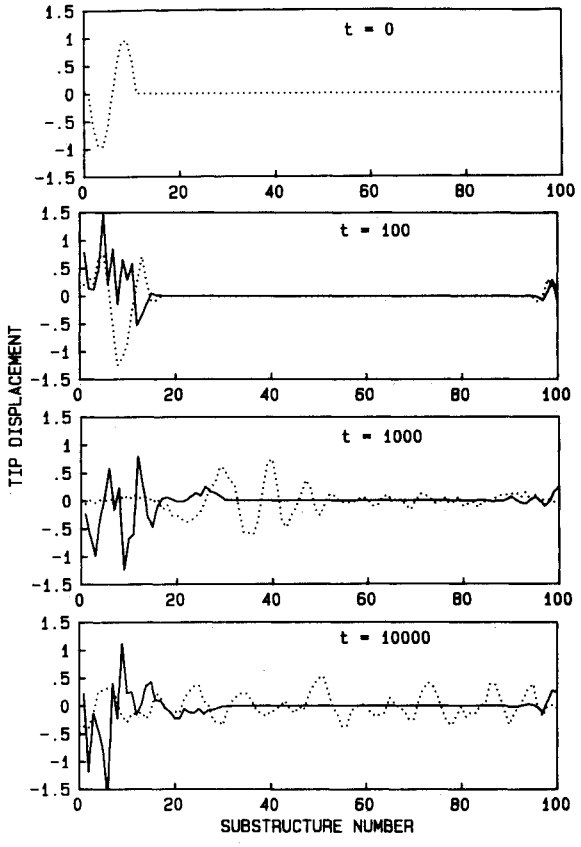

Fig. 13 Same as Fig. 12, except with 100 substructures. Note the large region where the substructure amplitudes remain negligible, indicating that the original wave packet is trapped.

For highly localized modes (extremely weak coupling), the location of the peaks can be predicted by inspecting the random variation associated with the rib flexural stiffness. The mode with the lowest natural frequency will have a peak at the rib with the lowest flexural stiffness, and so on. Once the peaks are aligned according to the natural frequencies of the individual ribs, a further increase in the imperfection level, or reduction of the coupling strength, will have no effect on the location of the peaks. As the imperfection strength is reduced, however, some of the natural frequencies appear to cross. Thus, at some levels of imperfection strength, the modes will be highly localized, only involving a few ribs, and yet will be in a location other than that predicted by looking at the individual ribs natural frequencies alone. Figure 10 is a trace of squared normalized frequency of the $n = 5$ and $n = 6$ modes of the third mode group. The symbols indicate the calculated values that were then connected by straight lines. The number in parentheses is the location of the primary peak or peaks in the associated natural mode. After doing extensive calculations to find the actual crossing point of these two modes, it was discovered that the natural frequencies get very close but actually *veer* away from each other, as shown in the expanded view in Fig. 10. The symbols are left off the expanded view for clarity. An important characteristic of curve veering is that the natural modes associated with the frequencies are exchanged during veering in a rapid but continuous way.[17] Figure 11 shows the mode shape for the $n = 5$ and $n = 6$ modes. Notice that a very small change in the imperfection strength alters the modes significantly around the veering point as the modes are exchanged.

Wave Confinement

Von Flotow[18] has shown that it may be advantageous to use the traveling wave approach when analyzing the dynamic behavior of large space structures. It is possible to define localization in terms of what happens to waves propagating along the structure. The effect of structural irregularities is then to cause multiple scattering or reflections of the waves at the substructure junctions. Localization is signaled by the structure becoming perfectly reflecting for certain wave modes, and the vibrational energy then becomes confined or "trapped" to a local region of the structure.

Hodges[2] has presented an analysis of this surprising phenomenon for a simple infinite one-dimensional structure, but his paper does not present supporting results from actual numerical experiments. Although the wave confinement can be understood in terms of multiple scattering of waves in an *infinite* structure, it appears almost counterintuitive for finite structures.

Figures 12 and 13 show results of calculations based on the simple structural model shown in Fig. 2 for $N = 40$ and $N = 100$, respectively. A sinusoidal wave is started over 10 of the substructures at $t = 0$, with initial conditions corresponding to a right-running wave. Since the coupling between the substructures is weak ($K_c/K = 1.0$, $K_h/K = 10$), it takes a relatively long time, between 100 and 1000 oscillation periods $T = 2\pi\sqrt{m/K}$, before the original "wave packet" has spread throughout the structure. When ±2.5% random imperfections are introduced in the substructure stiffness K, the vibratory behavior of the structure changes dramatically. In the case of 40 substructures (Fig. 12), the "wave packet" eventually spreads throughout the structure, although the amplitude remains small in a region of the structure away from the original 10 substructures. This is in contrast to the case of 100 substructures (Fig. 13), in which the vibratory energy remains confined to a well-defined local region of the structure. Calculations for $t = 10^6$ show that the wave is still confined, suggesting that the vibratory energy remains confined for all time. This confinement phenomenon was also observed when only one substructure was set in motion (plucked).

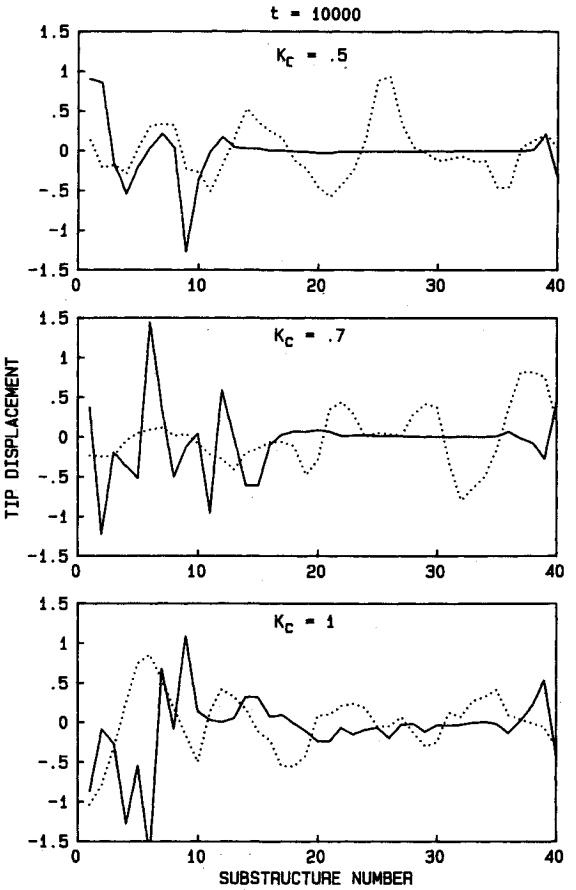

Fig. 14 Effect of coupling strength on the region of confinement. Same structure as in Fig. 12 ($N = 40$).

Figure 14 illustrates the effect of the coupling strength on the wave confinement phenomenon. As the coupling strength is increased, the region of activity also increases. This effect of K_c, as well as the effect of the number of substructures observed in Figs. 12 and 13, is in accordance with theoretical predictions.

Conclusions

1) For a generic class of large space reflectors with radial ribs, typical of proposed designs, certain of the vibratory modes will be quite sensitive to structural imperfections and, therefore, susceptible to localization.

2) For the 15-m-diam, 18-rib reflector studied, the first mode group did not localize, but the second and third mode groups did. The localization became progressively more severe with increasing mode number.

3) When the number of ribs was increased to 48, some of the modes in the first mode group did suffer severe distortion (or localization?), in contrast to the 18-rib case where only minor distortion was observed in the first mode group.

4) As the imperfection strength is increased from zero, some of the natural frequencies appear to cross, but actually veer away before crossing. Strong interactions are observed between the two modes, as indicated by the exchange in the localization peaks.

5) The surprising phenomenon of wave confinement by structural irregularities (expected in infinite structures) also appears to exist in finite engineering structures of practical interest.

Acknowledgments

The material presented in this paper is based upon work supported in part under a National Science Foundation Graduate Fellowship.

References

[1]Anderson, M. S., "Vibration and Buckling of General Periodic Lattice Structures," *Proceedings of the AIAA/ASME/ASCE/AHS 24th Structures, Structural Dynamics, and Materials Conference,* AIAA, New York, May 1984, pp. 206–213.

[2]Hodges, C. H., "Confinement of Vibration by Structural Irregularity," *Journal of Sound and Vibrations,* Vol. 82, No. 3, 1982, pp. 411–424.

[3]Bendiksen, O. O., "Aeroelastic Stabilization by Disorder and Imperfections," *Proceedings of the XVI International Congress of Theoretical and Applied Mechanics,* Lyngby, Denmark, Paper 583P, Aug. 1984.

[4]Pierre, C., "Analysis of Structural Systems with Parametric Uncertainties," Ph.D. Thesis, Dept. of Mechanical and Aerospace Engineering and Materials Science, Duke Univ., Durham, NC, July 1985.

[5]Bendiksen, O. O., "Mode Localization in Large Space Structures," *AIAA Journal,* Vol. 25, Sept. 1987, pp. 1241–1248.

[6]Pierre, C., Tang, D. M., and Dowell, E. H., "Localized Vibrations of Disordered Multispan Beams: Theory and Experiment," *AIAA Journal,* Vol. 25, Sept. 1987, pp. 1249–1257.

[7]El-Raheb, M. and Wagner, P., "Static and Dynamic Characteristics of Large Deployable Space Reflectors," *Proceedings of the AIAA/ASME/ASCE/AHS 22nd Structures, Structural Dynamics and Materials Conference,* AIAA, New York, April 1981, pp. 77–84.

[8]Belvin, W. K., "Vibration Characteristics of Hexagonal Radial Rib and Hoop Platforms," *Proceedings of the AIAA/ASME/ASCE/AHS 24th Structures, Structural Dynamics and Materials Conference,* AIAA, New York, May 1983, pp. 102–110.

[9]Gallagher, R. H., *Finite Element Analysis,* Prentice-Hall, Englewood Cliffs, NJ, 1975.

[10]Ishii, K., "Localization of Eigenstates and Transport Phenomena in the One-Dimensional Disordered System," *Progress in Theoretical Physics Supplement,* No. 53, 1973, pp. 77–138.

[11]Hodges, C. H. and Woodhouse, J., "Vibration Isolation from Irregularity in a Nearly Periodic Structure: Theory and Measurements," *Journal of the Acoustical Society of America,* Vol. 79, Sept. 1983, pp. 894–905.

[12]Borland, R. E., "The Nature of the Electronic States in Disordered One-Dimensional Systems," *Proceedings of the Royal Society,* Vol. A274, 1963, pp. 529–545.

[13]Hirota, T., "Degree of Localization for the Eigenstates in One-Dimensional Random Systems," *Progress in Theoretical Physics,* Vol. 50, Oct. 1973, pp. 1240–1247.

[14]Painter, R. D. and Hartmann, W. M., "Localization of the Vibrational States of Binary Disordered Linear Chains," *Physical Review B,* Vol. 13, Jan. 1976, pp. 479–491.

[15]Papatriantafillou, C., Economou, E. N., and Eggarter, T. P., "Eigenfunctions in One-Dimensional Disordered Systems I and II," *Physical Review B,* Vol. 13, Jan. 1986, pp. 910–928.

[16]Bendiksen, O. O. and Valero, N. A., "Localization of Natural Modes of Vibration in Bladed Disks," American Society of Mechanical Engineers, New York, Paper 87-GT-46, June 1987.

[17]Perkins, N. C. and Mote, C. D., "Comments on Curve Veering in Eigenvalue Problems," *Journal of Sound and Vibrations,* Vol. 106, No. 3, 1986, pp. 451–463.

[18]Von Flotow, A. H., "A Traveling Wave Approach to the Dynamic Analysis of Large Space Structures," *Proceedings of the AIAA/ASME/ASCE/AHS 24th Structures, Structural Dynamics and Materials Conference,* AIAA, New York, May 1983, pp. 509–519.